Published in final edited form as:
Dev Biol. 2008 November 1; 323(1): 6–18. doi:10.1016/j.ydbio.2008.08.019.

Development of the vertebral morphogenetic field in the mouse: interactions between Crossveinless-2 and Twisted gastrulation

Lise Zakin, **Carrie A. Metzinger**, **Ellen Y. Chang**, **Catherine Coffinier**, and **E. M. De Robertis***
Howard Hughes Medical Institute and Department of Biological Chemistry, University of California, Los Angeles, CA 90095-1662

Abstract

Crossveinless-2 (Cv2), Twisted Gastrulation (Tsg) and Chordin (Chd) are components of an extracellular biochemical pathway that regulates Bone Morphogenetic Protein (BMP) activity during dorso-ventral patterning of *Drosophila* and *Xenopus* embryos, the formation of the fly wing, and mouse skeletogenesis. Because the nature of their genetic interactions remained untested in the mouse, we generated a null allele for *Cv2* which was crossed to *Tsg* and *Chd* mutants to obtain *Cv2;Tsg* and *Cv2;Chd* compound mutants. We found that *Cv2* is essential for skeletogenesis as its mutation caused the loss of multiple bone structures and posterior homeotic transformation of the last thoracic vertebra. During early vertebral development, Smad1 phosphorylation in the intervertebral region was decreased in the *Cv2* mutant, even though CV2 protein is normally located in the future vertebral bodies. Because *Cv2* mutation affects BMP signaling at a distance, this suggested that CV2 is involved in the localization of the BMP morphogenetic signal. *Cv2* and *Chd* mutations did not interact significantly. However, mutation of Tsg was epistatic to all CV2 phenotypes. We propose a model in which CV2 and Tsg participate in the generation of a BMP signaling morphogenetic field during vertebral formation in which CV2 serves to concentrate diffusible Tsg/BMP4 complexes in the vertebral body cartilage.

Keywords

BMP; Crossveinless-2; Chordin; Twisted Gastrulation; Tolloid; vertebra; morphogenetic field; cartilage; pattern formation

Introduction

Pattern formation in the developing embryo is controlled by gradients of morphogens in which localization, local concentration, and binding to receptors must be precisely regulated. Extracellular protein-protein interactions ultimately determine how much signal is sensed by a cell at a specific position and its behavioral response within a morphogenetic field. The Bone Morphogenetic Protein (BMP) family of morphogens is involved in many developmental processes ranging from dorso-ventral patterning (De Robertis and Kuroda, 2004; Little and Mullins, 2006) to organogenesis and skeletal development (Hogan, 1996; Massague and Chen, 2000; Zhao et al., 2002). Central to the establishment of BMP morphogenetic gradients are the

*Author for correspondence: ederobertis@mednet.ucla.edu, Tel: (310) 206 1401; Fax: (310) 206 2008.

secreted BMP-binding proteins Chordin (Chd), Chordin-like-1 (Chdl-1), Chordin-like-2 (Chdl-2), Noggin, Twisted Gastrulation (Tsg) and Crossveinless-2 (CV2). Chd, Tsg and CV2 have been reported to function both as pro- and anti-BMPs depending on the model system studied (Little and Mullins, 2006; Oelgeschläger et al., 2000; Scott et al., 2001; Eldar et al., 2002; Nosaka et al., 2003; Coles et al., 2004; Petryk et al., 2004; Zakin and De Robertis, 2004; Ikeya et al., 2006; O'Connor et al., 2006; Zhang et al., 2007). Chdl-1 (Coffinier et al., 2001; Nakayama et al., 2001) and Chdl-2 (Nakayama et al., 2004; Zhang et al., 2007) are molecules that function as BMP antagonists in combination with Tsg, behaving similarly to Chd. The Chordin system is regulated by the Tolloid family of metalloproteinases that inactivate Chd by proteolytic cleavage and release previously inactive BMPs, which are then able to signal (Piccolo et al., 1997; Larrain et al., 2001).

Cv2 was first identified in *Drosophila* as a gene required for the formation of the wing crossveins, structures that require high BMP signaling (Conley et al., 2000; O'Connor et al., 2006; Blair, 2007). Mouse CV2 contains 5 cysteine-rich (CR) domains (also found in Chd, which function as BMP-binding modules) (De Robertis and Kuroda, 2004), a partial Von Willebrand Factor-D domain (vWFD), a trypsin inhibitor-like (TIL) domain involved in protein-protein interactions and/or oligomerization (Coffinier et al., 2001), and a heparin/extracellular matrix binding site within the vWFD domain that is thought to limit CV2 diffusion (Rentzsch et al., 2006; Serpe et al., 2008). The amino terminal domain of CV2 binds BMP, blocking the sites that are recognized by BMP receptors type I and II, thus preventing signaling (Zhang et al., 2008). One difference with Chd is that the *Cv2* gene product is constitutively secreted as two disulfide-linked fragments generated by an auto-catalytic cleavage occurring in the secretory pathway (Binnerts et al., 2004; Serpe et al., 2008; Ambrosio et al., 2008). Unlike Chd, vertebrate CV2 is completely resistant to digestion by Tolloid metalloproteinases (Ambrosio et al., 2008).

Both pro- and anti-BMP effects of CV2 have been reported depending on the experimental situation. Anti-BMP effects were described *in vitro* during the differentiation of endothelial cells (Moser et al., 2003), osteoblasts and chondrocytes (Binnerts et al., 2004). However, the co-transfection of *Cv2, Smad1* and *Bmp4* in Cos7 cells revealed a pro-BMP activity (Kamimura et al., 2004). The electroporation of *Cv2* in the neural tube of chick embryos produced pro-BMP phenotypes (Coles et al., 2004). In the mouse, *Cv2* has been reported to function as a pro-*Bmp4* in developing embryos (Ikeya et al., 2006). Likewise, pro-BMP effects were described in zebrafish embryos in morpholino knock-down experiments (Rentzsch et al., 2006; Moser et al., 2007). However, potent anti-BMP effects for CV2 were demonstrated in biochemical studies and in *Xenopus* and zebrafish overexpression experiments (Coles et al., 2004; Rentzsch et al., 2006; Zhang et al., 2007). In *Xenopus*, depletion of CV2 with morpholinos increased BMP signaling and strongly synergized with the depletion of the BMP antagonist *Chd*, indicating that the overall function of CV2 in early development is to inhibit BMP signaling (Ambrosio et al., 2008). Like Chd, CV2 binds directly to Tsg protein, which greatly increases its BMP inhibitory activity (Ambrosio et al., 2008).

In the fly wing, CV2 functions as a co-factor for Dpp/BMP that may concentrate the activity of this ligand in the crossvein. First, Dpp/Gbb BMP ligands form a diffusible complex with Sog/Chd and the dTsg-2/Cv-1 protein (Vilmos et al., 2005; Shimmi et al., 2005), and are subsequently released at the crossvein for signaling after cleavage of Sog by the Tolloid-related metalloproteinase Tlr (Ralston and Blair, 2005; Blair, 2007). Recent work by Serpe et al. (2008) has shown that CV2 also acts as a co-receptor that binds to Thickveins (Tkv, a Type I BMP receptor), facilitating BMP signaling at intermediate CV2 concentrations and inhibiting signaling at high CV2 concentrations. In the Drosophila wing, the CV2 secreted protein binds to the glypican Dally and stays locally, not signaling beyond one or two cell diameters from its site of synthesis (Serpe et al., 2008).

In the *Xenopus* gastrula, CV2 is expressed in the ventral (high-BMP) center. Biochemical studies have shown that mouse CV2 binds with high affinity (1 nM) to Chd protein, and even more strongly to Chd/BMP complexes or to Chd fragments resulting from cleavage of Chd by tolloids (Ambrosio et al., 2008). This led to the proposal that the pro-BMP effects of CV2 are caused by directing the flow of Tsg/Chd/BMP complexes towards more ventral regions in which CV2 is tethered to the cell surface (Ambrosio et al., 2008; Bier, 2008). The flow of BMP4 from dorsal toward ventral regions has been observed directly in the *Xenopus* gastrula, and shown to require endogenous Chd (Ben-Zvi et al., 2008). We now propose that a similar flow of Tsg/Chd/BMP4 toward prevertebral cartilage regions expressing CV2 protein at their surface might explain the formation of a BMP morphogenetic gradient during mammalian vertebral development.

In the present study we investigated the role of *Cv2* during mouse embryogenesis and its interactions with *Chd* and *Tsg* in controlling BMP signaling using mouse loss-of-function mutations. To analyze *Cv2* function *in vivo*, we inactivated the *Cv2* gene, characterized the mutant phenotype, and crossed heterozygous mice with the *Chd* (Bachiller et al., 2003) and *Tsg* (Zakin and De Robertis, 2004) mutant strains to generate compound *Cv2;Chd* and *Cv2;Tsg* mutants. We found that $Cv2^{-/-}$ pups died at birth (in agreement with Ikeya et al., 2006), of respiratory failure and displayed multiple skeletal abnormalities. Little or no interaction between *Cv2* and *Chd* was observed. Surprisingly, the $Cv2^{-/-}$ lethality and skeletal phenotype were completely suppressed in $Cv2^{-/-};Tsg^{-/-}$ double mutants. This rescue indicated that *Tsg* is epistatic over *Cv2*. The results also indicate that *Tsg*, *Cv2*, and possibly other BMP- and Tsg-binding proteins (such as Chdl-1, Chdl-2 and Chd), interact during skeletal development. We propose that the function of CV2 is to generate and maintain a BMP activity gradient in the developing vertebral morphogenetic field.

Materials and Methods

Generation of Cv2 mutant mice

Genomic DNA for *Cv2* recombination arms was isolated from a 129/SVJ mouse BAC library (Incyte Genomics) and subcloned into the pGN vector (Supplementary Fig. 1A) (Le Mouellic et al., 1990). The plasmid was electroporated into 129/SVJ ES cells and stable transfection was achieved after G418 selection. Clones were screened for homologous recombination by PCR using the following primers, CV2-5'2 (5'TCC ACC TTC TCA TTC ACA AC3') and CV2-3'2 (5'CGG GCC TCT TCG CTA TTA CG3') which yielded a diagnostic band of 2530 bp and homologous recombination was confirmed by Southern Blot (Supplementary Fig. 1B). The *Cv2* mutant strain was backcrossed into the hybrid strain B6SJLF1/J (Jackson Laboratories). The *Tsg* and *Chd* mutant strains were previously described (Bachiller et al., 2003; Zakin and De Robertis, 2004) and maintained in the same genetic background. The *Cv2, Tsg* and *Chd* mutant mouse strains used in this work are publicly available from Jackson Laboratories through an agreement made possible by the Howard Hughes Medical Institute (http://jaxmice.jax.org, stock numbers are 007552 for *Chd*, 007553 for *Tsg* and 007554 for *Cv2*).

Genotyping and RT-PCR

Genotyping of the *Cv2* mutant strain was performed by PCR (Supplementary Fig. 1A) using the following primers: pGN1 (5'ACC CTC TGT GTC CTC CTG TTA A3'), Cv2down (5'AGT CTC CTC CTA TGT TTC TTG C3') and Cv2up (5'TCT CTT TGG TGA TGC TAT TGT T3'). Tsg22 (5'AGC CTG AAT GTT TGA ATG TTT A3'), Tsg23 (5'CTT GAA TCC TTA CCT GAA TGA G 3') and LacZ3 (5'TCT GCC AGT TTG AGG GGA CGA C3') were used to genotype the *Tsg* mutant strain as previously described (Zakin et al ., 2004) and Neo2 (5'GTT CCA CAT ACA CTT CAT TCT CAG3'), Null Low (5'GGT AGG AGA CAG AGA AGC

GTA AAC T3') and Null Up2 (5'GAG TTA GGA GGT GGA GCT CTA CAC T3') for the *Chd* mutant strain (Bachiller et al., 2000).

For measuring transcripts by RT-PCR, the primers were RTCv2up (5'CTC CTT CCT GAC AGG GTC TG3') and RTCv2down (5'GGG TAC AAC CTT TGC ATC GT3') for *Cv2*, RTLacZdown (5'TTG AAA ATG GTC TGC TGC TG3') and RTlacZup (5'TAT TGG CTT CAT CCA CCA CA3') for *LacZ*, and HPRTforward (5'CAC AGG ACT AGA ACA CCT GC3') and HPRTreverse (5'GCT GGT GAA AAG GAC CTC T3') for HPRT. They yielded bands of 295 bp, 234 pb and 249 pb respectively.

In situ hybridization, histology, immunohistochemistry and skeletal preparations

Procedures for *in situ* hybridization on whole-mount and cryostat sections were as described (http://www.hhmi.ucla.edu/derobertis/) using the following probes: *Cv2* (Coffinier et al., 2002), *Tsg* (Zakin and De Robertis, 2004), *Chd* (Bachiller et al., 2000), *Chdl-1* (previously designated as *Neuralin 1*, Coffinier et al., 2001), *Chdl-2* (Genbank accession number AF 338222), and *Bmp1/Tll1* (Scott et al., 1999). Alcian Blue/Alizarin Red skeletal preparations, β-galactosidase, Hematoxylin and Eosin (H&E) and Mallory's tetrachrome stainings were as described (Zakin and De Robertis, 2004). For antibody staining, embryos were fixed in 4% paraformaldehyde in PBS, dehydrated, embedded in paraffin, serially sectioned at 7 μm and sections processed as described (http://www.hhmi.ucla.edu/derobertis/). Rabbit anti-pSmad1 (Cell Signaling #9511L) and anti-CV2 (R&D AF2299) antibodies were used at a 1:100 dilution.

Preparation of mouse embryonic fibroblasts (MEFs)

MEFs were prepared as previously described (Hogan et al., 1994), with the following modifications. 12.5 days post coïtum (d.p.c.) embryos were isolated from heterozygous mouse intercrosses. After head and viscera were removed, individual embryos were minced on a petri dish, using a sterile razor blade. 5 ml of trypsin (0.05%) was added to the minced tissue, transferred to a 15 ml falcon tube and incubated in 5% CO^2 at 37°C for 20 minutes. Trypsin was subsequently inactivated with 10 ml of DMEM/10% fetal calf serum (FCS). Cells from a single embryo were plated on a 10 cm tissue culture dish in DMEM/10% FCS.

Western blot analyses

Tissue or cell extracts were prepared in RIPA lysis buffer with a cocktail of phosphatase inhibitors (Complete-EDTA free from Roche and phosphatase inhibitor cocktail sets I and II from Calbiochem). Total-ERK (1:1000 dilution, Cell Signaling #9102), α-tubulin (1:1000, Calbiochem #CP06) and pSmad1 (1:1000 dilution, Cell Signaling #9511L) antibodies were used for western blot analyses. Quantitative analyses of the western blots in Fig. 7 and Supplementary Fig. 3 were performed with the Li-Cor Odyssey infrared imager using anti-mouse IRdye 680 (Li-Cor # 926-32220) and anti-rabbit IRdye 800 (Li-Cor # 926-32211) secondary antibodies at a dilution of 1:1500.

Results

Disruption of the Cv2 locus results in neonatal death and skeletal abnormalities

To investigate the role of *Cv2 in vivo* we generated a mutant allele of the mouse gene by inserting the reporter gene *LacZ* in frame at the initiation codon and deleting sequences between exon 1 and intron 2 (Supplementary Fig. 1). Loss of CV2 protein expression was confirmed by the absence of CV2 protein in prevertebral cartilages (compare Fig. 1A and A') and loss of *Cv2* transcript by RT-PCR on MEFs (Supplementary Fig. 1D). The *LacZ* reporter recapitulated the expression of endogenous *Cv2* in the tail bud, dorsal neural tube and brain dorsal midline

at 8.5–9.5 d.p.c. and in the branchial arches and heart at 9.5 d.p.c. (compare in Supplementary Fig. 1 panels E to E' and F to F').

Cv2$^{-/-}$ pups died at birth of respiratory failure. They displayed major skeletal abnormalities and shorter tails in all cases, and exencephaly with 25% penetrance (Fig. 1C–E' and Supplementary Fig. 2). The skeletal phenotypes were in agreement with the expression of CV2 protein in differentiating cartilage, such as the vertebral bodies and trachea (Fig. 1A, B and B'). The expression of *Cv2* in the brain dorsal midline (Supplementary Fig. 1E, E') correlated with the exencephaly phenotype. *Cv2*$^{-/-}$ mutants presented a dramatic reduction in the size of the vertebral bodies as well as neural arches of the vertebral column (Supplementary Fig. 2A, A', C–D'). The 13th thoracic vertebra displayed a posterior homeotic transformation characterized by the loss of the 13th rib with an almost complete penetrance (Supplementary Fig. 2C, C'). In the skull, a defective fusion of the basisphenoid bone and reduced ossification of the tympanic ring were present (Supplementary Fig. 2B, B'). Many of these bone phenotypes confirm those previously reported by the group of Yoshiki Sasai (Ikeya et al., 2006). We propose that respiratory failure is the most probable cause of the lethality, since the lumen of the trachea (Lt) was almost inexistent, compressed between the vertebral column and the manubrium sterni (Fig. 1 E-E'). This phenotype was caused by the absence of the tracheal cartilage rings that physically support the shape of the trachea (see insets in Fig. 1D and D') and express CV2 protein (Fig. 1B').

Expression patterns of Cv2, Tsg, Chd and Chdl-1 in the vertebral column

To better understand the *Cv2*$^{-/-}$ phenotype, the expression domain of *Cv2* was compared to those of other regulators of the BMP pathway, such as *Tsg, Chd, Chdl-1* and *Chdl-2*, which also bind to BMP4 (Oelgeschläger et al., 2000; Nakayama et al., 2004; Zhang et al., 2007). *In situ* hybridization on sections of 12.5 d.p.c. wild-type embryos using *Cv2, Tsg, Chd, Chdl-1* (Fig. 2A–D') and *Chdl-2* (not shown) probes, revealed that *Cv2* is expressed in the future vertebral bodies while *Tsg, Chd, Chdl-1* and *Chdl-2* are all expressed in the intervertebral disc region together with *Bmp4* (Zakin and De Robertis, 2004) and the Tolloid metalloproteinase *Bmp1/Tll1* (Fig. 4J and data not shown). As can be seen in the left hand side of panels 4A–D, these expression patterns were also similar at early prevertebral stages. In the *Drosophila* wing, the expression patterns for *Cv2*, *Chd/Sog*, *Bmp/Dpp* and *Bmp1/Tlr* are complementary: *Dpp* (*Decapentaplegic*) is present in the longitudinal veins, *Sog, Tlr, dTsg2* and *Gbb* (*glass bottom boat*, a BMP ligand) in the intervein regions, and CV2 protein is specifically localized to the crossveins, in which BMP signaling is maximal (Blair, 2007; Serpe et al., 2008). This suggested to us that other proteins made at a distance, such as Tsg, or the related proteins Chd, Chdl-1 and Chdl-2, might diffuse and interact with CV2 protein that remains anchored in the vertebral body cartilage in which it is transcribed (Fig. 1B and Fig. 2A, A').

CV2 regulates the phosphorylation state of Smad1 during vertebral development

To determine whether *Cv2* mutant phenotypes resulted from a pro- or anti-BMP activity of CV2, the levels of phosphorylated Smad1 (pSmad1), a direct downstream effector of BMP signaling, were analyzed in the differentiating vertebrae. Because the vertebral column forms sequentially (starting from the anterior), we compared in detail the histological structures, levels of Smad1 phosphorylation, and localization of CV2 protein at anterior and posterior locations (Fig. 3 and Fig. 4). In the posterior region of 12.5 d.p.c. embryos, the early vertebral column anlage is subdivided into uncondensed and condensed mesenchymes, which correspond to the future vertebral body and intervertebral disc, respectively (Fig. 3 A–F). No anatomical differences could be found at this stage in *Cv2*$^{-/-}$ compared to wild-type, but the peak of pSmad1 signal detected in the condensed mesenchyme was lost in the mutant (compare Fig. 3G to 3H). Surprisingly, the domain defective for Smad1 phosphorylation did not co-localize with the domain of highest CV2 protein expression (compare Fig. 3G to I). These

results indicated that CV2 is required to facilitate BMP signaling in a domain adjacent to, but not overlapping, the site of CV2 expression. One possible explanation could be that in *Cv2* mutants inhibitory Tsg/Chd/BMP4 or Tsg/Chdl/BMP4 complexes accumulate in the intervertebral region and are unable to signal. This would be in agreement with the finding that CV2 is a potent Chordin binding protein (Ambrosio et al., 2008) that would attract diffusing Chd/Tsg/BMP complexes to its site of expression in the future vertebral cartilage. These observations in the early developing vertebral field are summarized in Fig. 3J.

In the more developed anterior region of the 12.5 d.p.c. vertebral column, the vertebral bodies (in which CV2 is expressed) were reduced in $Cv2^{-/-}$ mutants (Fig. 4, panels C-F). The reduced vertebral body size might be explained by the failure to concentrate Tsg/Chd/BMP complexes in the vertebral cartilage (Ambrosio et al., 2008). The affected vertebral bodies coincided with maximal pSmad1 levels in both wild-type and $Cv2^{-/-}$ embryos. The area of pSmad1 signal was reduced in $Cv2^{-/-}$ (as was the cartilage), but was still clearly detected. At this more mature anterior level of the vertebral column, the expression of CV2 and pSmad1 proteins co-localized (compare Fig. 4G and I). A summary of these results is presented in Fig. 4J.

Biochemically, no significant differences were observed in total pSmad1 levels of whole tail extracts of wild-type and mutant 12.5 d.p.c. embryos (Fig. 5A). This might be explained by the presence in the tail of a heterogeneous population of multiple tissues at various stages of differentiation, thus diluting any differences in the levels of pSmad1.

BMP-inhibitory effects of CV2 in mutant MEFs

Because MEFs are of mesodermal origin, the same germ layer that is affected in $Cv2^{-/-}$ embryos, the effect of CV2 protein on BMP signaling was analyzed in the CV2 mutant background (Fig. 5B). Upon addition of 0.3 or 1 nM of BMP4 to $Cv2^{-/-}$ MEFs, Smad1 phosphorylation was induced in a dose-dependent manner (Fig. 5B, compare lanes 1, 3 and 5). This activation of pSmad1 was repressed by the addition of 1 nM CV2 protein (compare lanes 3 to 4 and 5 to 6). Note that CV2 inhibited BMP4 signaling even at equimolar amounts (Fig. 5B, lanes 5, 6). Similar inhibition of pSmad1 by CV2 protein was observed when wild-type MEFs were used (not shown). Importantly, the phosphorylation of Smad1 was higher in $Cv2^{-/-}$ MEFs compared to wild-type after addition of BMP4 (Fig. 5C, compare lanes 5 and 6). These experiments indicate that CV2 functions as an endogenous BMP signaling antagonist in fibroblasts in culture.

The pSmad1 staining in the developing vertebral column confirms that CV2 can have a pro-BMP activity *in vivo* in the future intervertebral disc (compare Fig. 3G and 3H, brackets). However, this occurs only at a distance from the CV2 protein expression site, suggesting that the defective BMP signaling phenotype results indirectly from a change in the activity of BMP signaling gradients. The CV2 protein remains anchored at its site of synthesis in the prevertebral body (Fig. 1B, 3I). In the absence of CV2 in vertebral bodies, inhibitory Tsg/Chd/BMP complexes may remain in the intervertebral region, resulting in the reduction in BMP signaling. In fibroblasts lacking *Cv2*, the response to BMP signaling was increased, suggesting that CV2 functions cell-autonomously as a BMP antagonist. These results may be explained through an interplay between CV2 and other BMP regulators (such as Tsg, Chd, Chdl-1 and Chdl-2) in the context of the flow of BMP-containing protein complexes in the developing vertebral morphogenetic field directed by CV2 protein (see discussion below).

We next analyzed pSmad1 levels in double mutant MEFs for CV2 and Chd. The response of $Cv2^{-/-}$, $Chd^{-/-}$, or $Cv2^{-/-};Chd^{-/-}$ MEFs to low levels of BMP4 (0.3 nM) was increased in all cases compared to fibroblasts from their wild-type siblings (Fig. 5C, lanes 5 to 8). Upon addition of increasing amounts of BMP4 protein, it was observed that $Cv2^{-/-};Chd^{-/-}$ double mutant MEFs showed a stronger BMP4 signaling response than wild-type MEFs at low BMP4

levels (0.1 and 0.3 nM) (Fig. 5D, lanes 3–6) but responded similarly at high BMP4 levels (1 nM) (Fig. 5D, lanes 7, 8). Please note that in all our MEF studies the effects of BMP4 addition on pSmad1 were analyzed after only 30 minutes of addition. Thus, our experiments reflect the initial BMP receptor activation and represent a direct readout of BMP4 signaling activity. These results in mutant MEFs show that the overall function of endogenous CV2 and Chd in fibroblasts is to serve as BMP4 antagonists. This is in agreement with loss-of-function studies in the *Xenopus* gastrula (Ambrosio et al., 2008).

A weak genetic interaction between Cv2 and Chd

We next investigated whether *Cv2* and *Chd* mouse mutants displayed genetic interactions. Mouse strains carrying the *Cv2* and *Chd* (Bachiller et al., 2003) mutations were crossed to generate $Cv2^{+/-};Chd^{+/-}$ mating pairs whose progeny was subsequently analyzed in late embryos before birth. Out of 159 embryos, all genotypes were recovered in the expected proportions except for the $Cv2^{+/-};Chd^{-/-}$ and $Cv2^{+/+};Chd^{-/-}$ embryos which were recovered in lower numbers than predicted by the mendelian ratio (Supplementary Table 1). This observation was in agreement with previous findings of early lethality in a small percentage of *Chd* mutants (Bachiller et al., 2003).

Bone formation is affected in both $Cv2^{-/-}$ and $Chd^{-/-}$ mutants and compound mutant skeletons were analyzed for possible interactions (Fig. 5E–H). Surprisingly, no significant effects were found in $Cv2^{-/-};Chd^{-/-}$ double mutants; in particular the characteristic posterior homeotic transformation of the 13th thoracic vertebra present in $Cv2^{-/-}$ was unaffected by the loss of Chordin (Fig. 5E–H). Conversely, the *Chd* mutant phenotype was unchanged by *Cv2* dosage. A weak recovery of the neural arches in the lumbar region of $Cv2^{-/-};Chd^{-/-}$ compared to $Cv2^{-/-};Chd^{+/+}$ was observed in some embryos (Fig. 5G, H and Supplementary Table 2), which would indicate opposing effects of CV2 and Chd. However, given that this weak rescue was limited to the lumbar neural arches, while the numerous other skeletal defects in both mutants showed no change, the functional significance of this interaction is difficult to evaluate. We propose that the lack of a strong interaction between *Cv2* and *Chd* in vertebral column development may be explained by the redundant anti-BMP activity of Chdl-1 and Chdl-2 molecules which have similar functions to Chd (Nakayama et al., 2001, 2004) and are co-expressed with Chd in the mouse (Fig. 2 and Fig. 4J). In conclusion, it is likely that uncovering a genetic interaction between *Cv2* and *Chd* will require simultaneous inactivation of *Chdl-1* and *Chdl-2*.

Mutation of Tsg suppresses Cv2 loss-of-function phenotypes, including lethality

We next analyzed the interaction between *Cv2* and *Tsg* in compound heterozygous knockout mice for *Cv2* (this work) and *Tsg* (Zakin and De Robertis, 2004). The genotype frequencies of the progeny of $Cv2^{+/-};Tsg^{+/-}$ intercrosses are presented in Table 1. Of 86 neonates, the $Cv2^{+/+};Tsg^{-/-}$ and $Cv2^{+/-};Tsg^{-/-}$ genotypes were obtained at slightly lower values than expected, perhaps due to an early lethality of $Tsg^{-/-}$ or to statistical error. $Cv2^{-/-};Tsg^{-/-}$ neonates were recovered in a higher percentage than expected (9%, 6.25% expected, n=8). More importantly, $Cv2^{-/-};Tsg^{-/-}$ pups survived, while all $Cv2^{-/-}$ neonates died at birth. When $Cv2^{-/-};Tsg^{-/-}$ skeletons were analyzed, they resembled $Tsg^{-/-}$ with most $Cv2^{-/-}$ skeletal phenotypes being rescued (Fig. 6). In all $Cv2^{-/-};Tsg^{-/-}$ neonates normal tracheal rings were present, probably explaining why the animals survive (compare Fig. 6B and D). The deltoid tuberosity of the humerus (compare Fig. 6F and H), the defects in the base of the skull (not shown), the neural arches (compare Fig. 6N and P), and the 13th rib lost in $Cv2^{-/-}$ (compare Fig. 6J and L) were all rescued in $Cv2^{-/-};Tsg^{-/-}$ animals. We conclude from these results that CV2 function requires Tsg, and that *Tsg* is epistatic to *Cv2*.

BMP signaling in $Cv2^{-/-};Tsg^{-/-}$ MEFs

We next tested whether *Tsg* was also epistatic in double mutants MEFs (Fig. 7A). In these experiments we used quantitative infrared Western blots using anti-rabbit pSmad1 in green for signaling and anti-mouse α-Tubulin in red as loading control. The signal intensities were measured in a Li-Cor infrared scanner, and histograms quantified pSmad1 signaling 30 min after addition of BMP4 are shown below each lane. Phosphorylated Smad1 levels were slightly higher in $Cv2^{-/-}$ fibroblasts compared to wild-type after the addition of 0.3 nM BMP4 (Fig. 7A, compare lanes 3 and 4). However, they were substantially reduced in $Cv2^{-/-};Tsg^{-/-}$ MEFs (Fig. 7A, compare lane 2 to 3 and 4), or in $Tsg^{-/-}$ single mutants (Fig. 7A, compare lane 2 to 1). Note that BMP signaling was impaired in $Tsg^{-/-}$ fibroblasts, demonstrating the pro-BMP effect of endogenous Tsg, and that this phenotype was dominant in $Cv2^{-/-};Tsg^{-/-}$ mutants (Figure 7A, see histograms for lanes 1 and 2).

To further study the interaction between *Cv2* and *Tsg*, the activities of these proteins was analyzed after addition to $Cv2^{-/-};Tsg^{-/-}$ MEFs (Fig. 7B). As previously noted, addition of CV2 protein to fibroblasts inhibited BMP signaling (Fig. 7B, compare lanes 2 and 3), while the simultaneous addition of 1 nM CV2 and Tsg lowered pSmad1 levels even more efficiently (Fig. 7B, lanes 3 and 5 and histogram below). We also tested the effect of the triple addition of CV2, Tsg and Chd proteins to $Cv2^{-/-};Tsg^{-/-}$ MEFs (Supplementary Fig. 3). This experiment indicated that when Chd, CV2 and BMP4 where added together, the inhibition of Smad1 phosphorylation was stronger than that obtained for CV2 or Chd alone (Supplementary Fig. 3, compare lane 7 to 4 and 6), indicating potent anti-BMP effects of CV2 in combination with Chd. Finally, when all the components (Tsg, CV2, Chd and BMP4) were present, the overall effect was an even stronger reduction of pSmad1 levels (Supplementary Fig. 3, compare lanes 2 and 9). In conclusion, the effect of simultaneous addition of Chd, CV2 and Tsg to fibroblasts lacking CV2 and Tsg is to inhibit BMP signaling.

In a different experimental design (Fig. 7C), CV2 protein was preincubated with the double mutant fibroblasts for 10 minutes, washed, and the supernatant replaced by medium containing BMP4 alone or BMP4 together with Tsg protein. In this experimental situation, the only CV2 present would be tethered to the cell surface (Fig. 7C). This setting should mimic better the *in vivo* situation in which CV2 serves as a co-receptor anchored at the cell surface (Serpe et al., 2008). While the reduction of BMP4 signaling levels by CV2 alone was less efficient in this experimental setting (Fig. 7C, compare lanes 2 and 3), the addition of Tsg and CV2 had a synergistic inhibitory effect on BMP4 signaling (Fig. 7C, compare lanes 3 and 5). This indicates that Tsg protein promotes the CV2 anti-BMP activity in fibroblasts, as it does in *Xenopus* embryos (Ambrosio et al., 2008).

Taken together, these results lead us to propose that the CV2 secreted protein helps establish morphogenetic fields of BMP signaling between intervertebral and vertebral regions of the vertebral column. In mouse fibroblasts, CV2 displays overall an anti-BMP activity. *In vivo*, CV2 would be required, in combination with Tsg, for the proper localization of the BMP morphogenetic signal to the vertebral cartilage.

Discussion

This study was undertaken to understand the role of CV2, Tsg and Chd interactions and their effect on BMP signaling during mouse embryogenesis. It was found that *Cv2* is essential for survival at birth and for proper skeletogenesis, in agreement with independent work of Ikeya et al. (2006). We propose that this skeletal phenotype is due to a defective localization of the BMP signal in the developing vertebral bodies, in which the CV2 protein is located. The most interesting observation reported here is that the lack of *Tsg* rescued most $Cv2^{-/-}$ phenotypes, including lethality (Fig. 6). We propose that the phenotype caused by the loss of *Cv2* is the

result of changes in Tsg activity, which functions in conjunction with other Tsg-binding proteins, such as Chd, Chdl-1 and Chdl-2 (Oelgeschläger et al., 2000; Nakayama et al., 2004; Zhang et al., 2007), to regulate the flow of BMP morphogenetic signals between the developing intervertebral and vertebral regions.

The biochemical functions of CV2 in embryos

Our understanding of the function of CV2 has been advanced by recent work (reviewed by Bier, 2008). In *Xenopus*, CV2 is expressed in the high-BMP region (ventral center) of the gastrula, where it functions as a local feedback inhibitor of BMP signaling (Ambrosio et al., 2008). Double knockdowns of CV2 and Chd present very high BMP signaling levels, and these suggested both proteins might interact. In biochemical studies CV2 was found to bind to Chordin with high affinity, and to Chordin/BMP or Chordin digestion products by tolloids with even higher affinity (Ambrosio et al., 2008). This led to the proposal that the pro-BMP effects of CV2 may be caused by directing the flow of Tsg/Chd/BMP complexes towards the ventral sites of CV2 expression (Ambrosio et al., 2008). The flow of BMP4 towards more ventral regions is known to require Chd in the *Xenopus* gastrula (Ben-Zvi et al., 2008). CV2 has an anti-Chd activity in *Xenopus*, since CV2 depletion causes the embryo to become hypersensitive to microinjected Chordin protein (Ambrosio et al., 2008). This suggests that cell surface CV2 may be involved in the clearing of Chd, or Chd degradation products, from the extracellular space. The net signaling effect of CV2 is dependent on the activity of the metalloproteinase Xolloid-related (Xlr) which cleaves Chd (but not CV2). In the absence of Xlr, CV2 removes BMP/Chd complexes, presumably by endocytosis, causing its anti-BMP effect. In the presence of Xlr, complexes of Tsg/Chd/BMP4, perhaps already bound to CV2, are clipped by Xlr, releasing BMP for peak signaling in the ventral side (Ambrosio et al., 2008).

In the *Drosophila* wing, CV2 is expressed in the crossveins, a region of peak BMP activity (Conley et al., 2000; Blair, 2006). The CV2 secreted protein remains tethered to its site of synthesis and does not diffuse more than two cell diameters, by virtue of its tight binding to a GPItethered heparin sulfate proteoglycan (HSPG) named Dally (Serpe et al., 2008). In zebrafish, CV2 also shows tight binding to HSPGs (Rentzsch et al., 2006). Importantly, CV2 also interacts with the BMP Type I receptor Thickveins (Tkv) (Serpe et al., 2008). This raises the intriguing possibility that CV2 may facilitate BMP signaling by bringing Dpp/Tsg2/Sog complexes in close proximity of BMP receptors (Serpe et al., 2008). In mammals, we have confirmed this interaction in vitro using commercial BMPR-1a (ALK-3) and CV2 proteins (A.L. Ambrosio and E.M.D.R., unpublished). It has been proposed that low levels of CV2 help deliver Dpp to Tkv, whereas high CV2 levels inhibit Dpp signaling in the crossvein (Serpe et al., 2008; Bier, 2008). Thus, both in vertebrates and in *Drosophila* profound strides have been made in unraveling how CV2, Tsg and Chd regulate the formation of BMP gradients.

Cv2 behaves as a local BMP antagonist in MEFs

The loss of CV2 resulted in multiple abnormalities in cartilages and bones of the skeleton (e.g. vertebrae, 13th rib, trachea, deltoid tuberosity of the humerus and basisphenoid). These defects may originate from the defective maturation of cartilage-producing cells (Ikeya et al., 2006). On the one hand, these phenotypes can be interpreted as decreased BMP signaling; in particular the loss of the 13th rib has been described in mutants for *Bmp4* (Lawson et al., 1999), *Bmp5* (Green and Green, 1946), *Bmp7* (Luo et al., 1995) and *Bmpr2* (Delot et al., 2003). Similarly, the loss of the deltoid tuberosity was observed in *Bmp7*$^{-/-}$*;Bmpr1b*$^{-/-}$ (Suzuki et al., 1996). The defects in vertebral neural arches could be attributed to either pro-or anti-BMP activities since they are observed in mutants for the BMP antagonist *Chd* (Bachiller et al., 2003), for the pro-BMP *Tsg* (Zakin and De Robertis, 2004) or for *Bmp7* (Jena et al., 1997).

We have derived *Cv2*$^{-/-}$*;Cv2*$^{-/-}$*;Chd*$^{-/-}$, and *Cv2*$^{-/-}$*Tsg*$^{-/-}$ MEFs that will be very useful to the field. We used these new reagents to examine the effect of the mutations on Smad1 phosphorylation 30 minutes after BMP addition. In fibroblasts in culture, the flow of BMP signals, as in intact embryos, should not play a functional role. When analyzed in culture, all single and double mutants indicated that CV2 behaved as an endogenous BMP antagonist in embryonic fibroblasts (Fig. 5 and Fig. 7). This is in agreement with the effect of morpholino depletions in *Xenopus*, in which Chd and CV2 are overall BMP antagonists (Ambrosio et al., 2008). In the case of *Tsg*$^{-/-}$ fibroblasts, or *Cv2*$^{-/-}$*;Tsg*$^{-/-}$ BMP signaling was reduced (Fig. 7A, lanes 1 and 2), supporting a pro-BMP function of Tsg (Oelgeschläger et al., 2000;Little and Mullins, 2006;Ambrosio et al., 2008). These results contrast with the report that *Cv2*$^{-/-}$ MEFs had reduced expression of cartilage markers 48 hours after BMP treatment (Ikeya et al., 2006). Since our measurements were performed 30 min after treatment we believe they represent a more direct readout of BMP signaling. Perhaps the results of the Sasai group are caused by binding of BMP, and Chd, to CV2 on the cell surface with subsequent release by tolloids after 48 hrs in tissue culture.

In conclusion, our *Cv2*$^{-/-}$ MEFs results as well as studies on the *Drosophila* wing (Ralston and Blair, 2005; Blair, 2007; Serpe et al., 2008) and the *Xenopus* gastrula (Ambrosio et al., 2008), suggest that the pro-BMP *Cv2* phenotypes may be caused by changes in BMP distribution in morphogenetic fields. The Chd-binding activity of CV2 would help generate a BMP gradient so that peak BMP signaling results from the diffusion of Tsg/Chd/BMP complexes from the intervertebral region towards the vertebral body where *Cv2* expression is high, serving to concentrate Tsg/Chd/BMP. Upon digestion of Chd by tolloid metalloproteinases, the released BMPs would be able to signal (Piccolo et al., 1997) while at low levels of tolloids CV2 would serve as a BMP antagonist by clearing Chd complexes (Ambrosio et al., 2008). In the *Drosophila* embryo, the flow of Dpp-GFP towards the dorsal midline of the *Drosophila* embryo has been documented (Wang and Ferguson, 2005), and shown to require endogenous Tsg/Sog/Dpp (Eldar 2002). Related observations have been made in *Xenopus* (Ben-Zvi et al., 2008).

We now propose a model in which the flow of BMP4-containing complexes towards CV2 expressing regions establishes a vertebral morphogenetic field. Although not yet tested directly, CV2 in the vertebral body might also concentrate the Chordin-like proteins, Chdl-1 and Chdl-2, produced in the intervertebral disc, which are also able to bind BMP4 and Tsg. We did not observe significant genetic interactions between *Cv2* and *Chd*, which may be explained by *Chdl-1* and *Chdl-2* activities which are redundant with *Chd* (Nakayama et al., 2004; Zhang et al., 2007).

The function of Cv2 in the vertebral column requires Tsg

In *Drosophila*, mutations in *dTsg2* (*Cv1*) or *Cv2* produce similar crossveinless phenotypes, indicating possible interaction between these molecules (Conley et al., 2000; Shimmi et al., 2005; Vilmos et al., 2005). In *Xenopus*, *Tsg* is strongly required for BMP signaling in *Cv2*-depleted embryos (Ambrosio et al., 2008). In the mouse, we now report a strong genetic interaction between *Cv2* and *Tsg* during development: all *Cv2*$^{-/-}$ skeletal phenotypes, and lethality, were rescued in *Cv2*$^{-/-}$*;Tsg*$^{-/-}$ animals, showing that *Tsg* is epistatic over *Cv2*. In the absence of Tsg, BMP provides only a local signal that manifests itself in the *Tsg*$^{-/-}$ phenotype (Nosaka et al., 2003; Petryk et al., 2004; Zakin and De Robertis, 2004). In *Cv2*$^{-/-}$*;Tsg*$^{-/-}$ double mutants the *Tsg* phenotype is epistatic because the other CR domain BMP-binding proteins - such as Chd, Chdl-1 and Chdl-2 - also require Tsg activity in order to contribute to the morphogenetic gradient.

In conclusion, the recent work in the *Drosophila* wing (Serpe et al., 2008) and the *Xenopus* gastrula (Ambrosio et al., 2008) support the view that CV2 functions to shape the Tsg/Chd/

BMP gradient. Tsg would be required for the expression of the *Cv2* phenotype because it is required for the flow of BMP4 complexes toward sites of CV2 expression. We propose, by analogy to the cases of the crossvein of the *Drosophila* wing and the *Xenopus* gastrula, that in the mammalian vertebral column the CV2/Chd/Tsg/BMP/Tolloid pathway may ultimately shape a morphogenetic field of BMP signaling that determines the choice between vertebral cartilage or intervertebral cell differentiation fates. This extracellular signaling network may contribute to the great evolutionary variability of vertebral morphology in the mammals. For example, the vast majority of mammals – including mice, humans and giraffes – have seven cervical vertebrae despite obvious differences in body size and shape.

Supplementary Material

Refer to Web version on PubMed Central for supplementary material.

Acknowledgements

The authors would like to thank D. Geissert and T. Boe for technical assistance and members of our laboratory for comments on the manuscript. The late Mario Zakin provided invaluable biochemical insights, R.I.P. Thanks to Dr. P. Perlman of the Howard Hughes Medical Institute for leadership in the public availability of our *Cv2*, *Tsg* and *Chd* mouse strains via the Jackson Laboratories. This work was supported by the Norman Sprague endowment (UCLA). E.M.D.R. is an investigator and L.Z. a research specialist of the Howard Hughes Medical Institute.

Appendix

Appendix A

Supplementary Figures 1–3 and Supplementary Table 1 and 2.

References

Ambrosio AL, Taelman VF, Lee HX, Metzinger CA, Coffinier C, De Robertis EM. Crossveinless-2 is a BMP feedback inhibitor that binds Chd/BMP to regulate *Xenopus* embryonic patterning. Dev Cell 2008;15:248–260. [PubMed: 18694564]

Bachiller D, Klingensmith J, Kemp C, Belo JA, Anderson RM, May SR, McMahon JA, McMahon AP, Harland RM, Rossant J, De Robertis EM. The organizer factors Chordin and Noggin are required for mouse forebrain development. Nature 2000;403:658–661. [PubMed: 10688202]

Bachiller D, Klingensmith J, Shneyder N, Tran U, Anderson R, Rossant J, De Robertis EM. The role of Chordin/BMP signals in mammalian pharyngeal development and DiGeorge syndrome. Development 2003;130:3567–3578. [PubMed: 12810603]

Ben-Zvi D, Ben-Zion S, Fainsod A, Barkai N. Scaling of the BMP activation gradient in *Xenopus* embryos. Nature 2008;453:1205–1211. [PubMed: 18580943]

Bier E. Intriguing extracellular regulation of BMP signaling. Dev. Cell 2008;15:176–177. [PubMed: 18694555]

Binnerts ME, Wen X, Cante-Barrett K, Bright J, Chen HT, Asundi V, Sattari P, Tang T, Boyle B, Funk W, Rupp F. Human Crossveinless-2 is a novel inhibitor of bone morphogenetic proteins. Biochem Biophys Res Commun 2004;315:272–280. [PubMed: 14766204]

Blair SS. Wing vein patterning in Drosophila and the analysis of intercellular signaling. Annu Rev Cell Dev Biol 2007;23:293–319. [PubMed: 17506700]

Coffinier C, Tran U, Larrain J, De Robertis EM. Neuralin-1 is a novel Chordin-related molecule expressed in the mouse neural plate. Mech Dev 2001;100:119–122. [PubMed: 11118896]

Coffinier C, Ketpura N, Tran U, Geissert D, De Robertis EM. Mouse Crossveinless-2 is the vertebrate homolog of a Drosophila extracellular regulator of BMP signaling. Gene Expr Patterns 2002;2:189–194. [PubMed: 12617799]

Coles E, Christiansen J, Economou A, Bronner-Fraser M, Wilkinson DG. A vertebrate crossveinless 2 homologue modulates BMP activity and neural crest cell migration. Development 2004;131:5309–5317. [PubMed: 15456729]

Conley CA, Silburn R, Singer MA, Ralston A, Rohwer-Nutter D, Olson DJ, Gelbart W, Blair SS. Crossveinless 2 contains cysteine-rich domains and is required for high levels of BMP-like activity during the formation of the cross veins in Drosophila. Development 2000;127:3947–3959. [PubMed: 10952893]

De Robertis EM, Kuroda H. Dorsal-Ventral Patterning and Neural Induction in Xenopus Embryos. Annu Rev Cell Dev Biol 2004;20:285–308. [PubMed: 15473842]

Delot EC, Bahamonde ME, Zhao M, Lyons KM. BMP signaling is required for septation of the outflow tract of the mammalian heart. Development 2003;130:209–220. [PubMed: 12441304]

Eldar A, Dorfman R, Weiss D, Ashe H, Shilo BZ, Barkai N. Robustness of the BMP morphogen gradient in Drosophila embryonic patterning. Nature 2002;419:304–308. [PubMed: 12239569]

Green EL, Green MC. Effect of the short ear gene on number of ribs and presacral vertebrae in the house mouse. Am Naturalist 1946;80

Hogan BL. Bone morphogenetic proteins: multifunctional regulators of vertebrate development. Genes Dev 1996;10:1580–1594. [PubMed: 8682290]

Hogan, BL.; Beddington, R.; Costantini, F.; Lacy, E. Manipulating the Mouse Embryo. Cold Spring Harbor, NY: Cold Spring Harbor Laboratory Press; 1994.

Ikeya M, Kawada M, Kiyonari H, Sasai N, Nakao K, Furuta Y, Sasai Y. Essential pro-Bmp roles of crossveinless 2 in mouse organogenesis. Development 2006;133:4463–4473. [PubMed: 17035289]

Jena N, Martin-Seisdedos C, McCue P, Croce CM. BMP7 null mutation in mice: developmental defects in skeleton, kidney, and eye. Exp Cell Res 1997;230:28–37. [PubMed: 9013703]

Kamimura M, Matsumoto K, Koshiba-Takeuchi K, Ogura T. Vertebrate crossveinless 2 is secreted and acts as an extracellular modulator of the BMP signaling cascade. Dev Dyn 2004;230:434–445. [PubMed: 15188429]

Larrain J, Oelgeschlager M, Ketpura NI, Reversade B, Zakin L, De Robertis EM. Proteolytic cleavage of Chordin as a switch for the dual activities of Twisted gastrulation in BMP signaling. Development 2001;128:4439–4447. [PubMed: 11714670]

Lawson KA, Dunn NR, Roelen BA, Zeinstra LM, Davis AM, Wright CV, Korving JP, Hogan BL. Bmp4 is required for the generation of primordial germ cells in the mouse embryo. Genes Dev 1999;13:424–436. [PubMed: 10049358]

Le Mouellic H, Lallemand Y, Brulet P. Targeted replacement of the homeobox gene Hox-3.1 by the Escherichia coli lacZ in mouse chimeric embryos. PNAS 1990;87:4712–4716. [PubMed: 1972279]

Little SC, Mullins MC. Extracellular modulation of BMP activity in patterning the dorsoventral axis. Birth Defects Res C Embryo Today 2006;78:224–242. [PubMed: 17061292]

Luo G, Hofmann C, Bronckers AL, Sohocki M, Bradley A, Karsenty G. BMP-7 is an inducer of nephrogenesis, and is also required for eye development and skeletal patterning. Genes Dev 1995;9:2808–2820. [PubMed: 7590255]

Massague J, Chen YG. Controlling TGF-beta signaling. Genes Dev 2000;14:627–644. [PubMed: 10733523]

Moser M, Binder O, Wu Y, Aitsebaomo J, Ren R, Bode C, Bautch VL, Conlon FL, Patterson C. BMPER, a novel endothelial cell precursor-derived protein, antagonizes bone morphogenetic protein signaling and endothelial cell differentiation. Mol Cell Biol 2003;23:5664–5679. [PubMed: 12897139]

Moser M, Yu Q, Bode C, Xiong JW, Patterson C. BMPER is a conserved regulator of hematopoietic and vascular development in zebrafish. J Mol Cell Cardiol 2007;43:243–253. [PubMed: 17618647]

Nakayama N, Han CE, Scully S, Nishinakamura R, He C, Zeni L, Yamane H, Chang D, Yu D, Yokota T, Wen D. A novel chordin-like protein inhibitor for bone morphogenetic proteins expressed preferentially in mesenchymal cell lineages. Dev Biol 2001;232:372–387. [PubMed: 11401399]

Nakayama N, Han CY, Cam L, Lee JI, Pretorius J, Fisher S, Rosenfeld R, Scully S, Nishinakamura R, Duryea D, Van G, Bolon B, Yokota T, Zhang K. A novel chordin-like BMP inhibitor, CHL2, expressed preferentially in chondrocytes of developing cartilage and osteoarthritic joint cartilage. Development 2004;131:229–240. [PubMed: 14660436]

Nosaka T, Morita S, Kitamura H, Nakajima H, Shibata F, Morikawa Y, Kataoka Y, Ebihara Y, Kawashima T, Itoh T, Ozaki K, Senba E, Tsuji K, Makishima F, Yoshida N, Kitamura T. Mammalian twisted gastrulation is essential for skeleto-lymphogenesis. Mol Cell Biol 2003;23:2969–2980. [PubMed: 12665593]

O'Connor MB, Umulis D, Othmer HG, Blair SS. Shaping BMP morphogen gradients in the Drosophila embryo and pupal wing. Development 2006;133:183–193. [PubMed: 16368928]

Oelgeschläger M, Larrain J, Geissert D, De Robertis EM. The evolutionarily conserved BMP-binding protein Twisted gastrulation promotes BMP signalling. Nature 2000;405:757–763. [PubMed: 10866189]

Oelgeschläger M, Reversade B, Larrain J, Little S, Mullins MC, De Robertis EM. The pro-BMP activity of Twisted gastrulation is mediated by inhibition of Chordin-like BMP-binding modules. Development 2003;130:4047–4056. [PubMed: 12874126]

Petryk A, Anderson RM, Jarcho MP, Leaf I, Carlson CS, Klingensmith J, Shawlot W, O'Connor MB. The mammalian twisted gastrulation gene functions in foregut and craniofacial development. Dev Biol 2004;267:374–386. [PubMed: 15013800]

Piccolo S, Agius E, Lu B, Goodman S, Dale L, De Robertis EM. Cleavage of Chordin by Xolloid metalloprotease suggests a role for proteolytic processing in the regulation of Spemann organizer activity. Cell 1997;91:407–416. [PubMed: 9363949]

Ralston A, Blair SS. Long-range Dpp signaling is regulated to restrict BMP signaling to a crossvein competent zone. Dev Biol 2005;280:187–200. [PubMed: 15766758]

Rentzsch F, Zhang J, Kramer C, Sebald W, Hammerschmidt M. Crossveinless 2 is an essential positive feedback regulator of Bmp signaling during zebrafish gastrulation. Development 2006;133:801–811. [PubMed: 16439480]

Scott IC, Blitz IL, Pappano WN, Maas SA, Cho KW, Greenspan DS. Homologues of Twisted gastrulation are extracellular cofactors in antagonism of BMP signalling. Nature 2001;410:475–478. [PubMed: 11260715]

Serpe M, Umulis D, Ralston A, Chen J, Olson DJ, Avanesov A, Othmer H, O'Connor MB, Blair SS. The BMP binding protein Crossveinless 2 is a short-range, concentration-dependant, biphasic modulator of BMP signaling in Drosophila. Dev Cell 2008;14:940–953. [PubMed: 18539121]

Shimmi O, Ralston A, Blair SS, O'Connor MB. The crossveinless gene encodes a new member of the Twisted gastrulation family of BMP-binding proteins which, with Short gastrulation, promotes BMP signaling in the crossveins of the Drosophila wing. Dev Biol 2005;282:70–83. [PubMed: 15936330]

Suzuki N, Labosky PA, Furuta Y, Hargett L, Dunn R, Fogo AB, Takahara K, Peters DM, Greenspan DS, Hogan BL. Failure of ventral body wall closure in mouse embryos lacking a procollagen C-proteinase encoded by Bmp1, a mammalian gene related to Drosophila tolloid. Development 1996;122:3587–3595. [PubMed: 8951074]

Vilmos P, Sousa-Neves R, Lukacsovich T, Marsh JL. crossveinless defines a new family of Twisted-gastrulation-like modulators of bone morphogenetic protein signalling. EMBO Rep 2005;6:262–267. [PubMed: 15711536]

Wang YC, Ferguson EL. Spatial bistability of Dpp-receptor interactions during *Drosophila* dorsal-ventral patterning. Nature 434:229–234. [PubMed: 15759004]

Zakin L, De Robertis EM. Inactivation of mouse Twisted gastrulation reveals its role in promoting Bmp4 activity during forebrain development. Development 2004;131:413–424. [PubMed: 14681194]

Zhang JL, Huang Y, Qiu LY, Nickel J, Sebald W. von Willebrand factor type C domain-containing proteins regulate bone morphogenetic protein signaling through different recognition mechanisms. J Biol Chem 2007;282:20002–20014. [PubMed: 17483092]

Zhang ZL, Qiu LY, Katzsch A, Weidauer S, Patterson L, Hammerschmidt M, Sebald W, Mueller TD. Crystal Structure analysis reveals how the Chordin family member crossveinless 2 blocks BMP-2 receptor binding. Dev Cell 2008;5:739–750. [PubMed: 18477456]

Zhao M, Harris SE, Horn D, Geng Z, Nishimura R, Mundy GR, Chen D. Bone morphogenetic protein receptor signaling is necessary for normal murine postnatal bone formation. J Cell Biol 2002;157:1049–1060. [PubMed: 12058020]

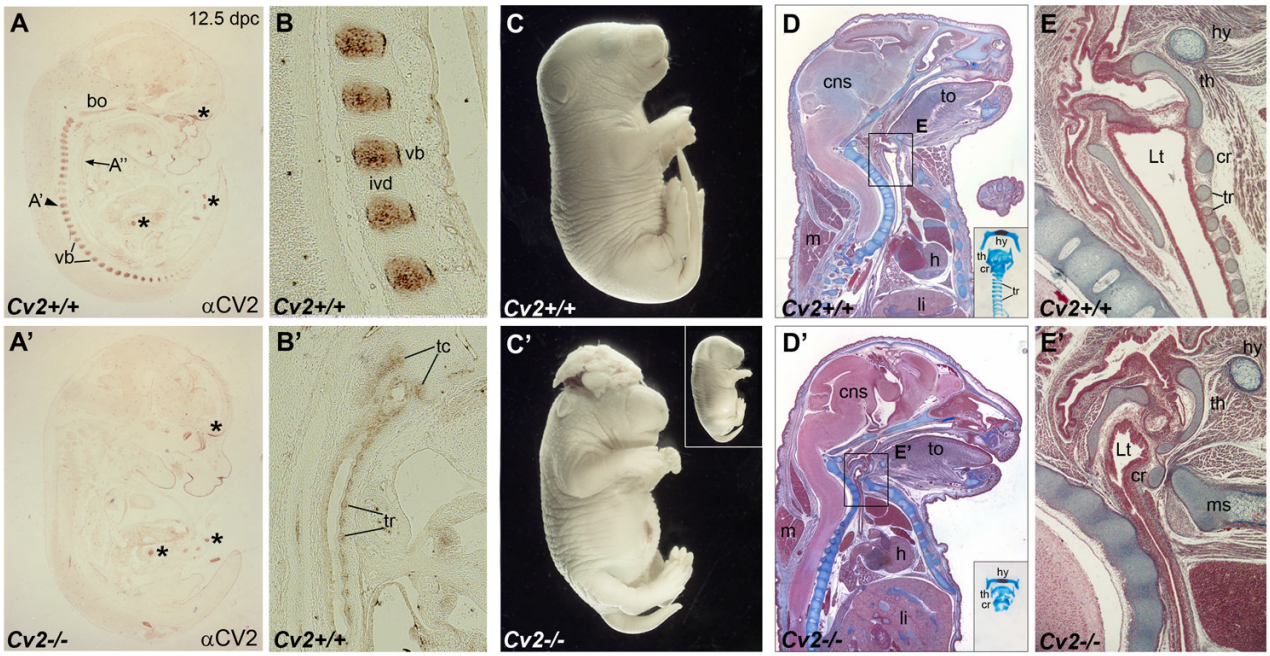

Fig. 1.

CV2 expression pattern at 12.5 d.p.c. and *Cv2*$^{-/-}$ phenotype. (A-A') Detection of the CV2 protein on sagittal paraffin sections of wild-type and *Cv2* mutant mouse embryos at 12.5 d.p.c. by immunohistochemistry. Note in wild-type the CV2 protein staining in the vertebral bodies (vb). No CV2 protein is detected in *Cv2*$^{-/-}$ embryos. Asterisks indicate unspecific signals present in both wild-type and mutant embryos. bo, basioccipital bone. (B) Higher magnification view of the CV2 staining in the vertebral bodies. ivd, intervertebral disc. (B') The CV2 signal in thyroid cartilages (tc) and tracheal rings (tr), shown at a higher magnification. (C-C') External view of littermates from *Cv2*$^{+/-}$ intercrosses showing shorter tails in *Cv2*$^{-/-}$ compared to wild-type and exencephaly observed in 25% of the mutants. Inset shows a *Cv2*$^{-/-}$ mutant lacking exencephaly. (D-E') Mallory's tetrachrome staining of sagittal paraffin sections of wild-type (top panels) and mutant (bottom panels) neonates. *Cv2*$^{-/-}$ embryos die at birth of respiratory failure. Note in the thoracic region of *Cv2*$^{-/-}$ the reduction of the lumen of the trachea and the decreased distance between the vertebral column and the manubrium of the sternum (ms). Insets show tracheas of wild-type and *Cv2*$^{-/-}$ embryos stained with Alcian Blue and Alizarin Red. Note that in the mutant the cartilage rings that support the trachea are absent. Boxed areas are shown at higher magnification in (E) and (E'). In the mutant the collapse of the tracheal lumen (Lt) is due to the absence of the tracheal rings (tr). cns, central nervous system; cr, cricoid cartilage; h, heart; hy, hyoid bone; li, liver; m, muscle; th, thyroid cartilage ; to, tongue.

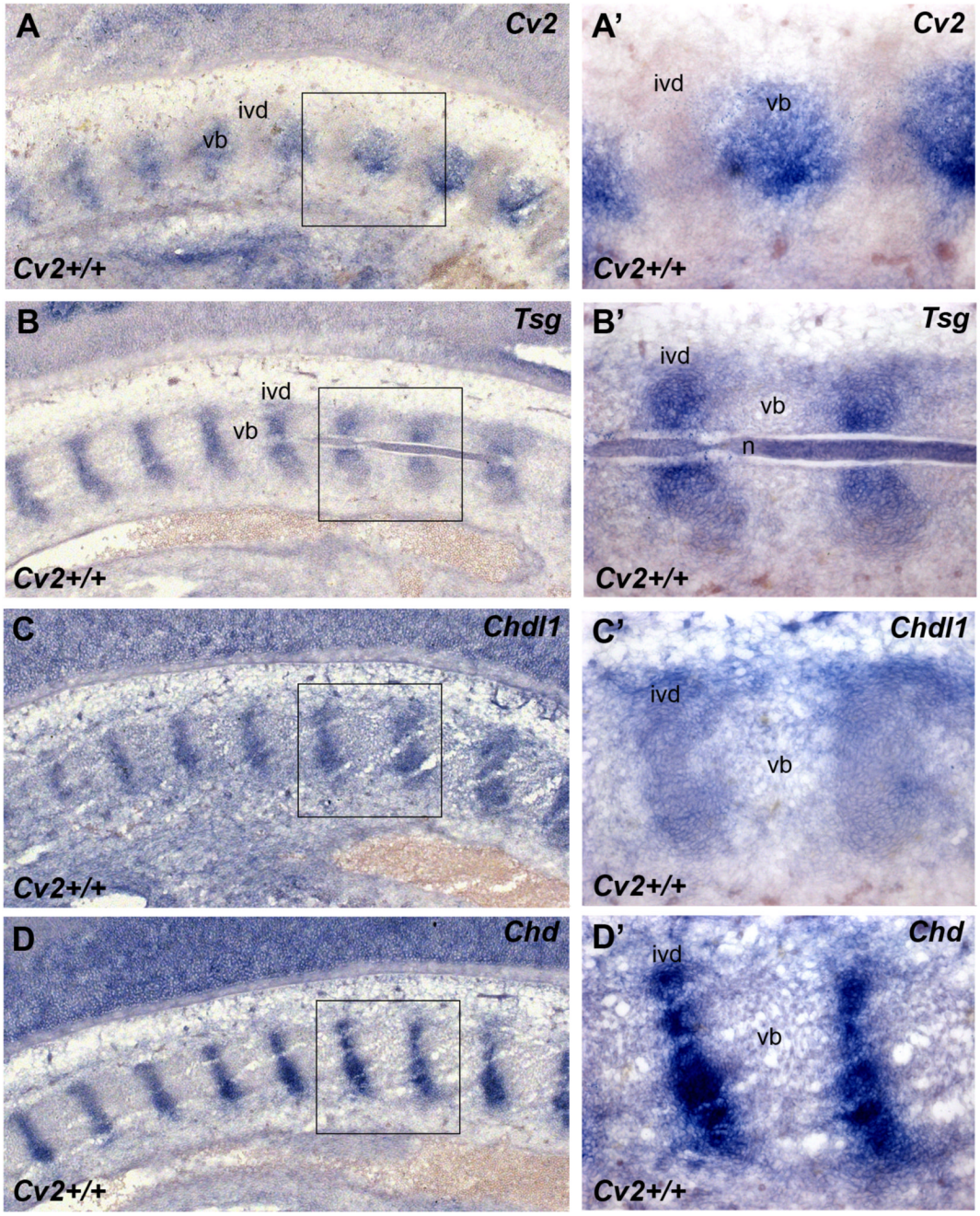

Fig. 2.

Pattern of expression of genes containing BMP-binding CR modules in the mouse vertebral column. (A–D') *Cv2* is expressed in a pattern complementary to that of *Tsg, Chdl-1* and *Chd* in the vertebral column of 12.5 d.p.c. embryos. *In situ* hybridization on cryostat sections. Boxed areas in A, B, C, D are shown at higher power in A', B', C', D', respectively. *Cv2* mRNA is expressed in the vertebral body (vb) (A, A') while *Tsg* (B, B'), *Chdl-1* (C, C') and *Chd* (D, D') all co-localize in the intervertebral disc (ivd).

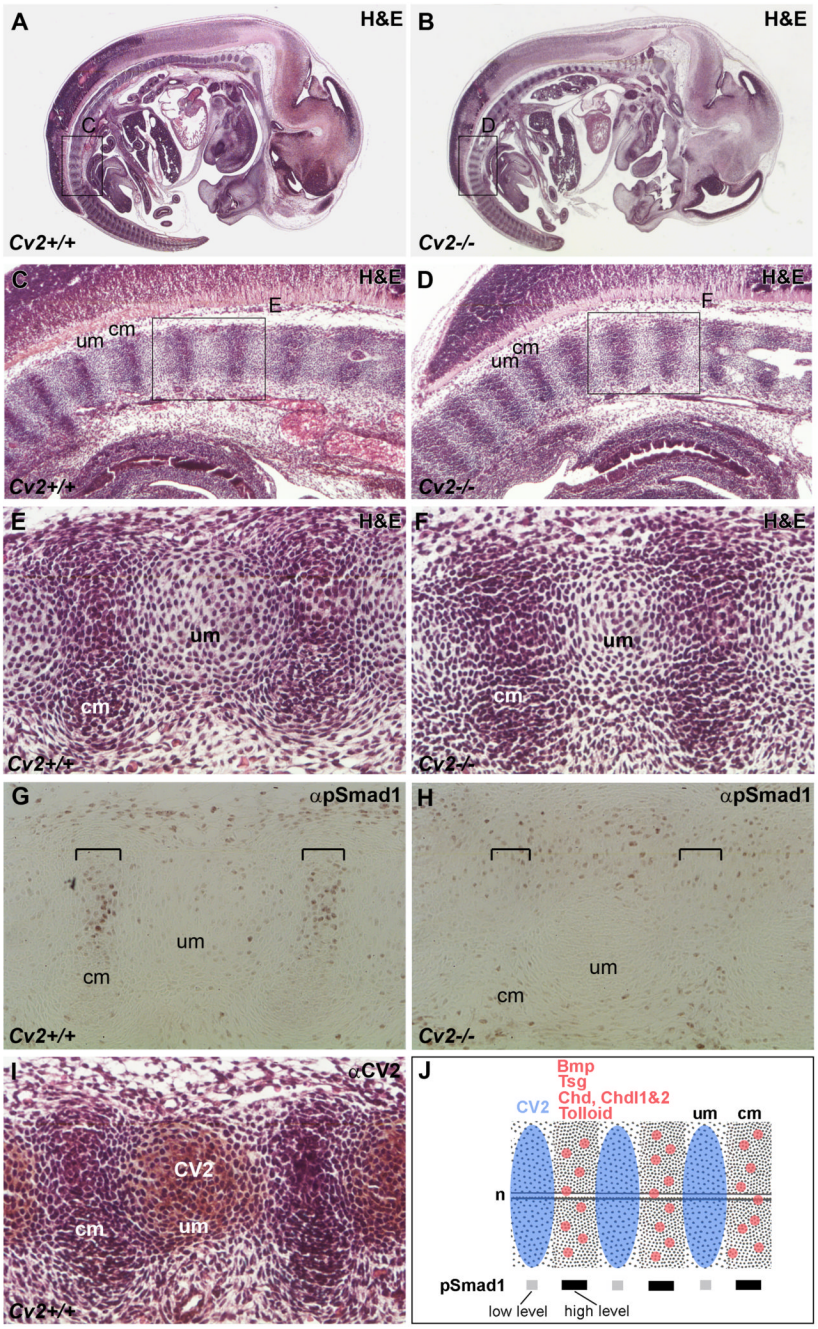

Fig. 3.

Smad1 phosphorylation in the developing pre-vertebral region of *Cv2*$^{-/-}$ 12.5 d.p.c. embryos (posterior, more immature regions are shown). Sagittal paraffin sections of wild-type (A, C, E, G, I) and *Cv2*$^{-/-}$ (B, D, F, H) 12.5 d.p.c. embryos. (A, B) Sections stained with H&E. Boxed areas are shown at higher magnification below. (C–F) H&E staining revealed no morphological differences between wild-type and mutant embryos in this posterior region. cm, condensed mesenchyme (prospective intervertebral disc); um, uncondensed (intervertebral) mesenchyme (prospective vertebral body). (G, H) Detection of phosphorylated Smad1 (pSmad1) by immunohistochemistry. pSmad1 was detected at higher levels in the condensed (intervertebral) mesenchyme (indicated by brackets in G); however, this signal was lost in the mutant (brackets

in H). (I) Detection of CV2 protein by immunohistochemistry in sections counterstained with H&E. Note that the localization of the CV2 protein in the uncondensed mesenchyme (future vertebral body) is complementary to the pSmad1 domain at this stage. (J) Summary of the expression of CV2 protein compared to *Bmp*, *Tsg*, *Chd*, *Chdl-1*, *Chdl-2* and *Tolloid* mRNAs and to pSmad1 levels in the posterior vertebral column. The highest levels of pSmad1 overlap with *Bmp*, *Tsg*, *Chd Chdl-1*, *Chdl-2* and *Tolloid* in the cm (future intervertebral region), and are complementary to the domain of CV2 expression in the um (prospective vertebral body). n, notochord.

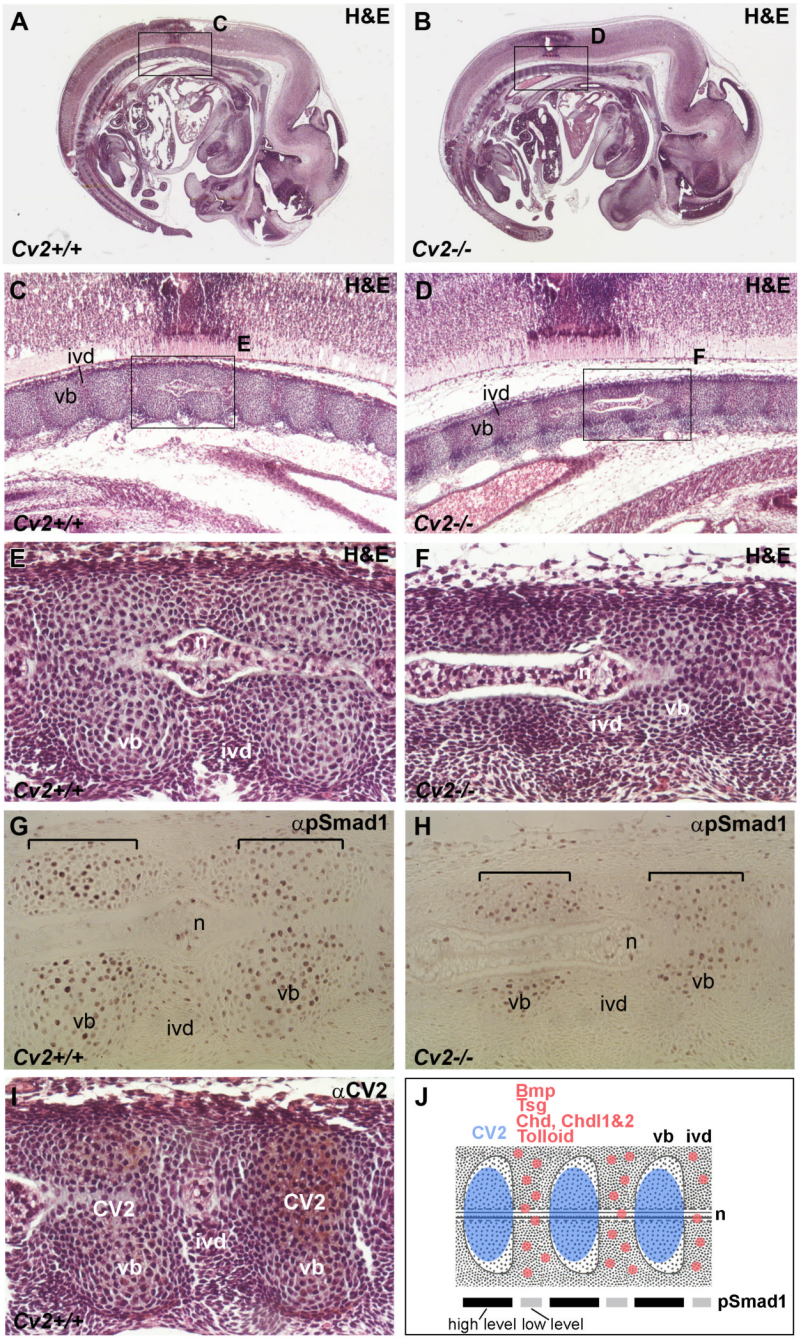

Fig. 4.

Impaired vertebral body differentiation in *Cv2*$^{-/-}$ 12.5 d.p.c. embryos (anterior, more mature vertebral regions are shown). Sagittal paraffin sections of wild-type (A, C, E, G, I) and *Cv2*$^{-/-}$ (B, D, F, H) 12.5 d.p.c. embryos. (A, B) Sections stained with H&E. Boxed areas are shown at higher power in (C, D and E, F). Vertebral bodies (vb) are smaller in the mutant, while the intervertebral discs (ivd) appear to be unaffected.n, notochord. (G, H) pSmad1 is detected at higher levels in the vb at this stage. In *Cv2*$^{-/-}$ mutants the area stained for pSmad1 (brackets) is smaller than in the wild-type, reflecting the reduced size of the vertebral body. (I) Detection of CV2 protein by immunohistochemistry in sections counterstained with H&E. CV2 is present in the vb, co-localizing with pSmad1. (J) Summary of the expression of CV2

protein compared to that of *Bmp, Tsg, Chd, Chdl-1, Chdl-2* and *Tolloid* mRNAs and to pSmad1 levels in the anterior vertebral column. At this stage the highest levels of pSmad1 co-localize with CV2 protein in the vb and are complementary to the expression domain of *Bmp, Tsg, Chd Chdl-1, Chdl-2* and *Tolloid* mRNAs in the ivd.

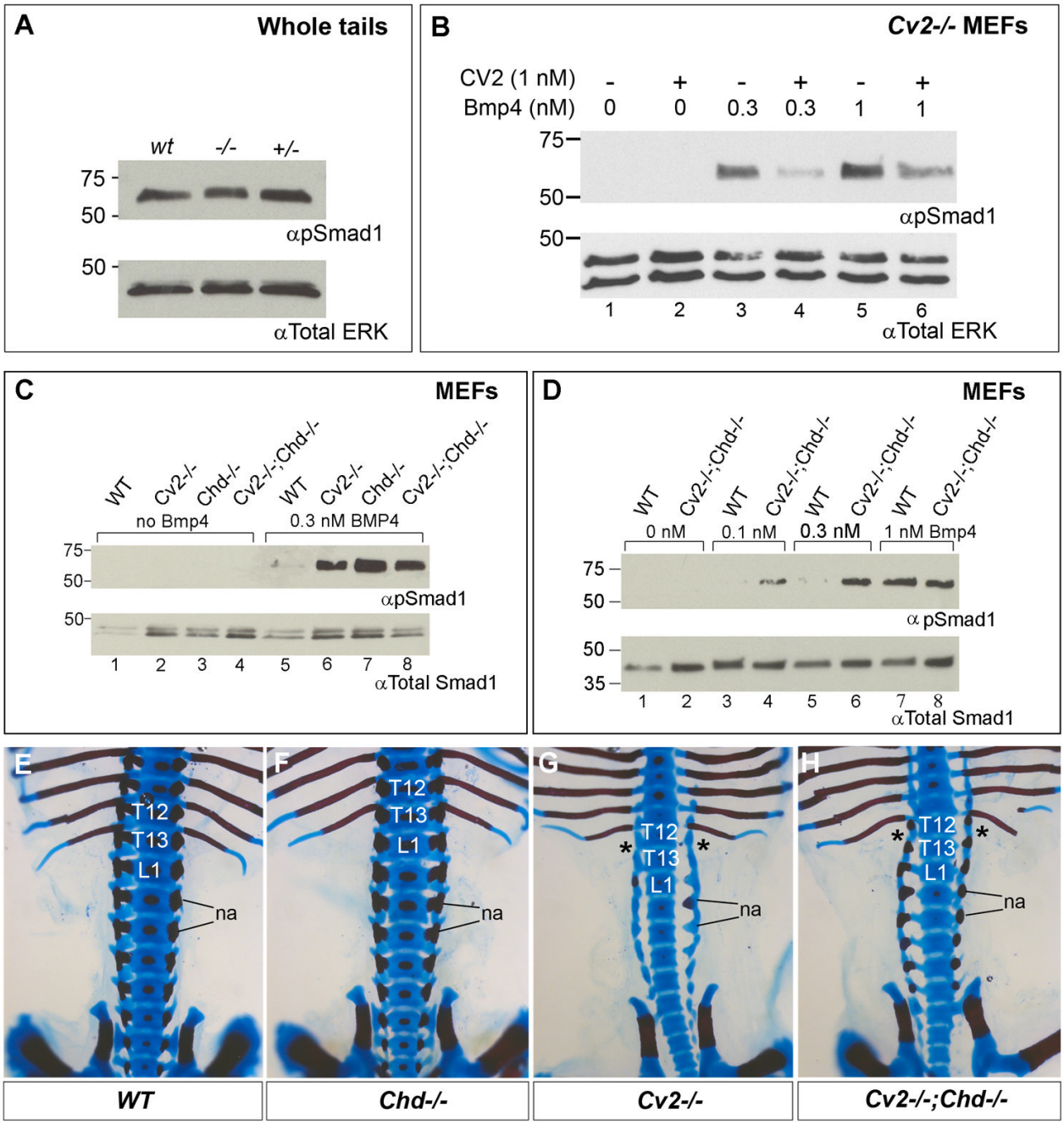

Fig. 5.

Western blot analyses of Smad1 phosphorylation in whole tails, MEFs derived from wild-type, *Cv2*$^{-/-}$, *Chd*$^{-/-}$ and *Cv2*$^{-/-}$;*Chd*$^{-/-}$ treated with BMP4 protein, and lack of skeletal genetic interactions between *Cv2* and *Chd* mutants. (A) Western blot showing comparable amounts of endogenous Smad1 phosphorylation in tails from wild-type, *Cv2*$^{-/-}$ and *Cv2*$^{+/-}$ 12.5 mouse d.p.c. embryos. The tail contains multiple tissues in addition to the vertebral column which is the topic of this study. No significant differences in pSmad1 are seen. (B) Addition of purified CV2 protein to *Cv2*$^{-/-}$ MEFs inhibits Smad1 phosphorylation induced by 30 min treatment with BMP4. (C) pSmad1 levels are higher in *Cv2*$^{-/-}$, *Chd*$^{-/-}$ and *Cv2*$^{-/-}$;*Chd*$^{-/-}$ MEFs compared to wild-type fibroblasts upon addition of 0.3 nM of BMP4 (compare lane 5 to lanes

6–8). (D) pSmad1 response levels are higher in *Cv2*$^{-/-}$;*Chd*$^{-/-}$ MEFs compared to wild-type at low amounts of BMP4 (compare lanes 3 to 4, and 5 to 6. (E–H) Genetic interaction between *Cv2* and *Chd* in the lumbar region of the vertebral column. Bone is stained with Alizarin Red and cartilage with Alcian Blue. Dorsal view of the skeletons of wild-type (E), *Chd*$^{-/-}$ (F), *Cv2*$^{-/-}$ (G) and *Cv2*$^{-/-}$;*Chd*$^{-/-}$ (H) neonates. In this region the skeleton of *Chd*$^{-/-}$ (F) is indistinguishable from wild-type (E). The posterior homeotic transformation indicated by the loss of the 13th rib (asterisk) is present in *Cv2*$^{-/-}$ and *Cv2*$^{-/-}$;*Chd*$^{-/-}$ embryos. na, neural arches.

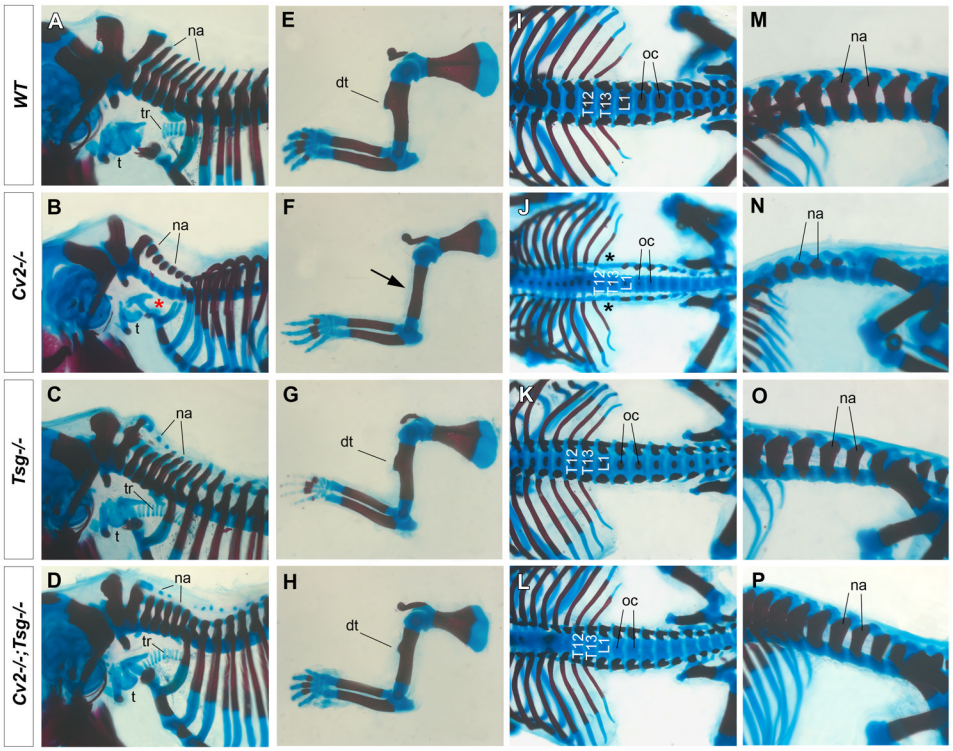

Fig. 6.

Tsg is epistatic over *Cv2*: the loss of *Tsg* in $Cv2^{-/-}$ suppresses most of the *Cv2* mutant skeletal phenotypes. Skeletal preparations of wild-type (A, E, I, M), $Cv2^{-/-}$ (B, F, J, N), $Tsg^{-/-}$ (C, G, K, O) and $Cv2^{-/-};Tsg^{-/-}$ (D, H, L, P) neonates stained with Alizarin Red and Alcian Blue. (A–D) The cervical neural arches (na) are reduced in $Cv2^{-/-}$ but are rescued in $Cv2^{-/-};Tsg^{-/-}$ double mutants. The tracheal rings (tr) are missing in $Cv2^{-/-}$ (red asterisk in B), but the tracheal (t) cartilage develops like wild-type (A) in $Cv2^{-/-};Tsg^{-/-}$ double mutants (D). (E–H). $Cv2^{-/-}$ lack the humerus deltoid tuberosity (dt), which is rescued in $Cv2^{-/-};Tsg^{-/-}$. (I–L) The posterior homeotic transformation of T13 (black asterisks) in $Cv2^{-/-}$ (J) is rescued in $Cv2^{-/-};Tsg^{-/-}$ (L); however the ossification centers (oc) remain defective. (M–P) Side views of the lumbar region. Neural arches (na) are reduced in $Cv2^{-/-}$ (N) but are only mildly affected in $Cv2^{-/-};Tsg^{-/-}$ (P), as is the case in $Tsg^{-/-}$ mutants (O).

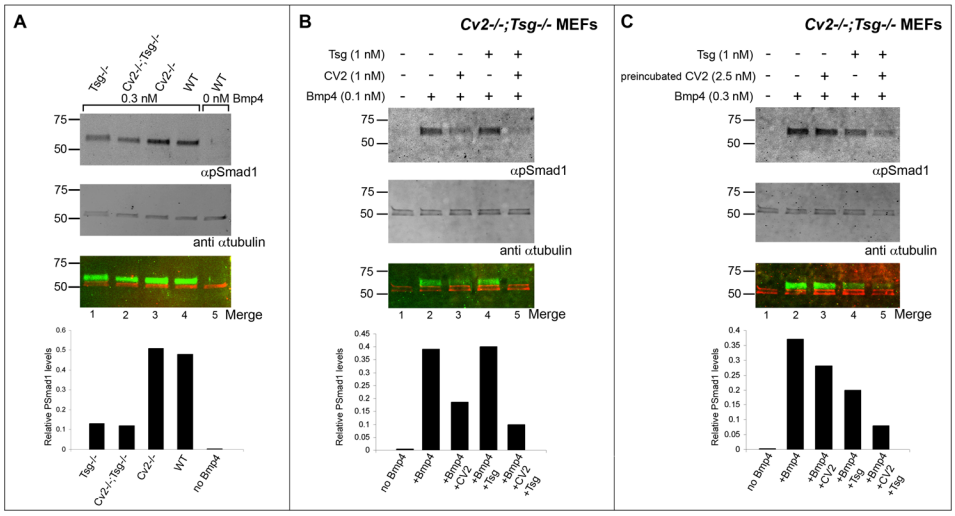

Fig. 7.

Western blot analyses of Smad1 phosphorylation in *Cv2*$^{-/-}$;*Tsg*$^{-/-}$ double mutant MEFs. Signals generated by infrared conjugated secondary antibodies were detected using the Li-Cor Odyssey imager. In the bottom blot, the artificial colors red and green correspond to signals detected at λ680 nm (anti-mouse secondary antibody against the αTubulin antibody used here as loading control) and 800 nm (anti-rabbit secondary antibody against the pSmad1 antibody), respectively. The infrared imager system allows quantification of the relative pSmad1 levels with respect to total protein loading and this is shown in the histograms at the bottom of the blots. (A) pSmad1 levels are reduced in *Tsg*$^{-/-}$ and *Cv2*$^{-/-}$;*Tsg*$^{-/-}$ MEFs when compared with *Cv2*$^{-/-}$ or wild-type fibroblasts upon addition of 0.3 nM of BMP4, indicating that BMP4 signaling is impaired in the absence of *Tsg* (pro-BMP effect of Tsg) and that this is not affected by removal of CV2. (B) Effects of exogenous CV2 and Tsg on BMP4 signaling in *Cv2*$^{-/-}$;*Tsg*$^{-/-}$ MEFs. Simultaneous addition of CV2 and Tsg proteins inhibited BMP signaling more efficiently than CV2 alone, demonstrating that Tsg promotes the anti-BMP effects of CV2. (C) Experiments in which CV2 was preincubated with *Cv2*$^{-/-}$;*Tsg*$^{-/-}$ MEFs for 10 minutes and subsequently washed to remove excess CV2, leaving only CV2 bound to the cell surface. Note that the inhibition of BMP signaling was stronger in the presence of Tsg preincubated with BMP4 (anti-BMP effect of Tsg).

Table 1

Suppression of the *Cv2*$^{-/-}$ lethal phenotype by *Tsg* loss-of-function. Genotypes of neonates obtained from *Cv2*$^{+/-}$;*Tsg*$^{+/-}$ intercrosses.

Genotype	Number of Embryos	Observed percentage (Expected Percentage)	Number of embryos with *Cv2* skeletal phenotype* (%)
Cv2$^{+/+}$; *Tsg*$^{+/+}$	8	9 (6.25)	
Cv2$^{+/-}$; *Tsg*$^{+/+}$	12	14 (12.5)	
Cv2$^{+/+}$; *Tsg*$^{+/-}$	9	10.5 (12.5)	
Cv2$^{+/-}$; *Tsg*$^{+/-}$	23	27 (25)	
Cv2$^{+/+}$; *Tsg*$^{-/-}$	4	5 (6.25)	
Cv2$^{+/-}$; *Tsg*$^{-/-}$	8	9 (12.5)	
Cv2$^{-/-}$ ***; Tsg***$^{+/+}$ **	5	6 (6.25)	**5 (100%)**
Cv2$^{-/-}$ ***; Tsg***$^{+/-}$ †	9	10.5 (12.5)	**8 (90%)**
Cv2$^{-/-}$ ***; Tsg***$^{-/-}$ ‡	8	9 (6.25)	**0 (0%)**
Total	86		

* *Cv2* skeletal phenotypes include lack of the 13th rib and deltoid tuberosity, skull phenotype, and absence of the tracheal rings. Because defective neural arches and shorter tails are also found in *Tsg* mutants, this phenotype was not taken into account in this table.

** all died as neonates

† most died as neonates

‡ some of these animals were recovered alive at day 3 post-partum; since these *Cv2*$^{-/-}$;*Tsg*$^{-/-}$ mutants displayed the *Tsg*$^{-/-}$ skeletal phenotype we conclude that *Tsg* is genetically epistatic over *Cv2*. The rescue of the *Cv2*$^{-/-}$ phenotype in *Cv2*$^{-/-}$;*Tsg*$^{-/-}$ was found to be statistically significant using a chi-square test for independence ($p<0.001$).